Giant, 17, 2024, 100231

Full-length article

Thiol-ene click chemistry incorporates carboxylic acid-terminated alkane pendants on polycyclooctene to tune properties

Eli Fastow[a,1], **Roshni John Chethalen**[b,1], **E. Bryan Coughlin**[b,*], **Karen I. Winey**[a,c,*]

[a] Department of Materials Science and Engineering, University of Pennsylvania, Philadelphia, PA 19104, United States
[b] Department of Polymer Science and Engineering, University of Massachusetts Amherst, Amherst, Massachusetts 01003, United States
[c] Department of Chemical and Biomolecular Engineering, University of Pennsylvania, Philadelphia, Pennsylvania 19104, United States

Keywords: Polymer upcycling, Thiol-ene click chemistry, Polycyclooctene, Associating polymer, Functionalization, Dynamic mechanical analysis

Dehydrogenation and subsequent chemical modification of polyolefins emerges as a promising polymer-to-polymer upcycling pathway. We report the functionalization of polycyclooctene (PCOE), a model for dehydrogenated polyethylene, by thiol-ene click chemistry to install carboxylic acid (COOH) terminated alkane pendant groups. This functionalization approach attached three pendants of different alkane spacer length: thioglycolic acid, mercaptopropionic acid, and mercaptooctanoic acid. Functionalization attached pendants to 3–22 mol% of the ethylene monomeric units, was well controlled by varying reaction stoichiometry and time, and did not require acid groups protections. Greater than 95% of the COOH groups participated in secondary bonding, forming aggregates detectable in X-ray scattering at high COOH mass fractions. Crystallinity and melting temperature decreased with increasing COOH mass fraction. Dynamic mechanical analysis (DMA) reveals both COOH mass fraction and pendant architecture tunes the rubbery plateau moduli, which is well described by the molar mass per backbone bond. This functionalized polymer exhibits commensurate surface and mechanical properties to commercial poly(ethylene-*co*-acrylic acid).

Introduction

Though plastics offer significant value in modern life, managing their waste poses a tremendous environmental challenge. The U.S. recycled < 8% of the 51 million tons of plastic waste it created in 2021, a stark illustration of the challenges unmet by conventional recycling technologies [1–3]. Conventional mechanical recycling alters the molecular weight distribution of polyolefins, degrading properties and reducing the material value by a factor of >2 when compared to pristine polymer [4–6]. Given this limit inherent to conventional recycling approaches, chemical recycling has drawn significant interest as it transforms waste polymer into higher value products [1,4]. Ultimately, valorization of polymer waste will become necessary to reduce the total environmental impact of plastics [7].

* Corresponding authors.
E-mail addresses: coughlin@mail.pse.umass.edu (E.B. Coughlin), winey@seas.upenn.edu (K.I. Winey).
Received 17 August 2023; Received in revised form 11 December 2023; Accepted 23 December 2023
[1] Both Eli J. Fastow and Roshni John Chethalen contributed equally to the manuscript.

https://doi.org/10.1016/j.giant.2023.100231

Polymer-to-polymer chemical recycling and upcycling target the conversion of waste polymer to higher value polymers [1]. This both consumes polymer waste and creates specialty polymers without needing to use petrochemical feedstock [7,8]. Polymer-to-polymer upcycling has been investigated with direct functionalization of waste polymer by metal catalysis, organocatalysis, free radical generators, and xanthylation among other approaches [9–13]. Alternatively, we propose dehydrogenating waste polyethylene (PE) as the first step of polymer-to-polymer upcycling followed by functionalization to preserve molar mass. Prior work from both the Goldman and Coates groups have already demonstrated dehydrogenation of polyolefins to generate unsaturations [14–16]. More recent work also used dehydrogenation as part of a pathway to deconstruct polyolefins [17–19]. As polyolefins constitute over 57% of global plastic production and are currently recycled at low rates, developing a successful upcycling pathway represents an opportunity to recover value from materials that are currently thrown away [1].

In prior work, we demonstrated thiol-ene click chemistry to functionalize polycyclooctene (PCOE) with hydroxyl ethyl thioether pendant groups [20]. Thiol-ene click chemistry proceeds under mild conditions either neat or in benign solvents under UV light to install functionality on vinyl groups [21,22]. This reaction was used to functionalize polybutadiene by Coughlin et al., and was applied to upcycling of poly(acrylonitrile butadiene styrene) polymers by Kim et al. [21,23]. We functionalized PCOE as a model for upcycling partially-dehydrogenated polyethylene (PE), Fig. 1**a**. In our prior work we demonstrated both good control over the level of functionalization and that the extent of pendant incorporation tunes thermal, structural, surface, and adhesive properties [20]. Herein we further elaborate on the use of thiol-ene click chemistry to functionalize PCOE with carboxylic acid (COOH) terminated linear alkane pendants.

Polyolefin copolymers with carboxylic acid functionality, e.g. poly(ethylene-*co*-acrylic acid) (EAA) or poly(ethylene-*co*-methacrylic acid) (EMA), are well studied and commercially important for their broad range of tunable surface, mechanical, and rheological properties [24–27]. The inclusion of acid groups reduces the crystallinity and forms nanoscale aggregates of hydrogen-bonding acid groups [24,26–29]. These acid aggregates act as physical crosslinks, and give rise to the properties typically valued in associating polymers, including high toughness, high surface polarity, and resistance to flow. Conventional acid-containing polymers are prepared by high pressure free radical polymerization resulting in a highly branched architecture with a random distribution of acids [24]. The relationships between acid concentration in conventional acid-containing polymers and key properties, including thermal, dynamic, rheological, and mechanical, are well studied [25,27,30–34]. These material properties are typically described with multi-component models to include amorphous and crystalline domains [28,30,31,35,36]. Wakabayashi and Register first applied the Davies model that describes total elastic modulus as a combination of contributions from the amorphous and crystalline domains to EAA [31]. Prior studies by Winey have investigated the role of acid aggregates on mechanical and dynamic behavior in precise acid-containing

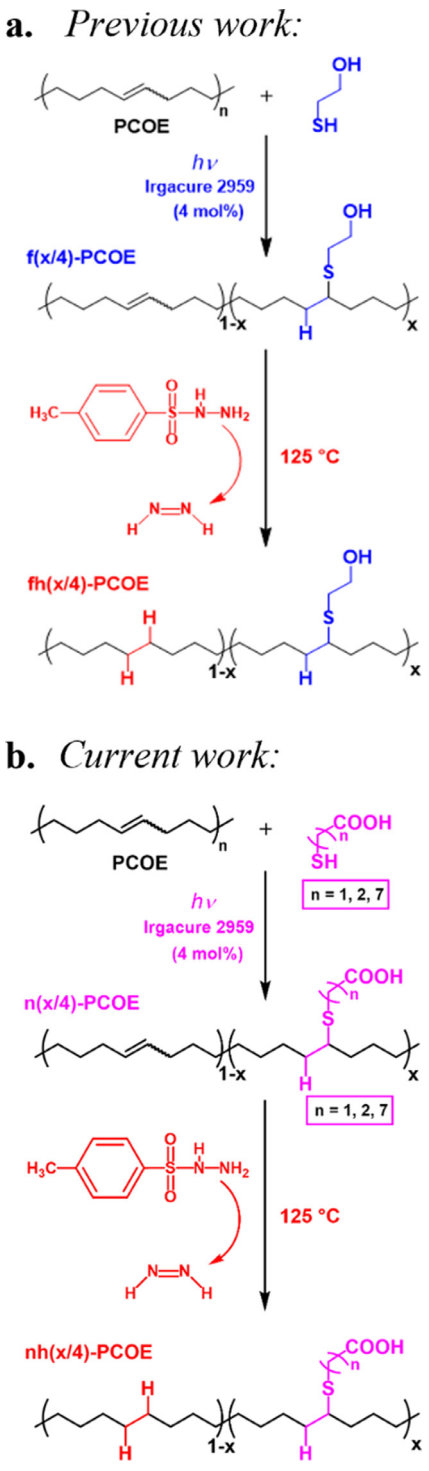

Fig. 1

(a) Partial functionalization of PCOE with mercaptoethanol and subsequent hydrogenation, previously reported [20]. **(b)** Partial functionalization of PCOE with carboxylic acid terminated alkane pendants followed by hydrogenation of the functionalized product.

polymers through X-ray scattering, tensile testing, quasi-elastic neutron scattering, and molecular dynamics simulations [37–42]. Precise EAA polymers synthesized by acyclic diene metathesis (ADMET) exhibit unique mechanical behavior. For example, at intermediate acid content (~ 26 wt% COOH), the acid aggregates

transform from liquid-like distribution to layers, driving strain hardening [39]. Thus, synthesizing precise or pseudo-precise acid-containing polymers via different routes is also of interest.

Herein, we design thiol-ene click chemistry to generate novel acid-containing polymers with linear alkane pendant groups with carboxylic acid and investigate their structure-property relationships. An alkane spacer separates the carboxylic acid from the backbone. Starting with PCOE, we synthesized novel functional polymers with methylene spacers of 1, 2 or 7 carbons. We show good control over the level of functionalization through both the thiol:vinyl ratio and reaction time. This versatile chemistry also works with polyolefins at lower levels of unsaturation, as demonstrated here by the functionalization of partially-hydrogenated PCOE. Notably, this functionalization approach does not require steps to protect and de-protect the carboxylic acids, an improvement over previously reported approaches to synthesizing precise acid-containing polymers [37,43].

We characterized the structural, thermal, dynamic mechanical, and surface properties as a function of acid concentration and spacer length. The sulfur radical addition to the C=C to create a thio-ether is not regio-regular, and therefore the pendant groups at full functionalization are, on average, separated by 6, 7, or 8 methylene units. Thus, at high levels of functionalization, the acid-PCOE materials become pseudo-precise, allowing us to identify acid aggregates in X-ray scattering [39]. This work demonstrates a route to synthesizing pseudo-precise acid-containing polymers with unusual and tunable properties. We find a strong dependence on acid concentration for all properties, though only select behaviors depend on the spacer length including the glass transition and melting temperatures. The rubbery plateau modulus decreases at higher molar mass per backbone bond. Notably, these polymers exhibit both surface and mechanical properties commensurate with commercial EAA, demonstrating promise for applications in packaging.

Experimental methods

Materials

The following reagents were purchased from various vendors and used as received. *cis*-Cyclooctene (contains 100–200 ppm Irganox 1076 FD as antioxidant, 95%), dichloromethane (CH_2Cl_2, >99%), cis-1,4-Dibenzyloxy-2-butene ($C_6H_5CH_2OCH_2CH{=}CHCH_2OCH_2C_6H_5$, 95%), Grubbs Catalyst® M300 ($C_{38}H_{40}Br_2Cl_2N_4Ru$), methanol ($CH_3OH$, ACS grade), tetrahydrofuran (THF, ACS grade), thioglycolic acid ($HSCH_2COOH$), mercaptopropionic acid ($HS(CH_2)_2COOH$), mercaptooctanoic acid ($HS(CH_2)_7COOH$), *p*-toluenesulfonyl hydrazide (TSH, $C_7H_{10}N_2O_2S$, 97%), p-xylene ($C_6H_4(CH_3)_2$, 99%), 1,1,2,2-Tetrachloroethane (TCE, $C_2H_2Cl_4$, 98%), Dimethyl sulfoxide (DMSO, $(CH_3)_2SO$, 99%), Tri-*n*-propyl amine (TPA, $(CH_3CH_2CH_2)_3$ N, ≥98%). The UV lamp was purchased from cureuv.com 16 inch (406 mm) mountable UV lamp with UV-A 36 Watt bulb emitting ultraviolet light with wavelengths of 315–400 nm. Commercial EAA was purchased from Sigma Aldrich with COOH concentrations of 5 and 15 wt% as reported by the vendor. These polymers were prepared by free radical polymerization, and therefore have high dispersity and are branched [44].

Functionalization of PCOE using thiogycolic acid

PCOE with benzyloxy end-groups was synthesized following a procedure described in a previous publication [20]. In a 20 ml vial, 750 mg of PCOE (M_n = 11,200 g/mol by ^{1}H NMR, 0.07 mmoles) was dissolved in 15 ml of THF at room temperature. The solution was degassed with an N_2 purge for 10 min after which thioglycolic acid (thiol to vinyl ratio 2:1) was added to the solution. After sparging with nitrogen for 5 more minutes, Irgacure 2959 (2 mol% relative to vinyl) was added to the solution. The reaction vial was sealed and stirred while exposed to UV-A light for either 15, 30, 60, 100, and 120 min to attain different levels of functionalization. The reaction solution was then precipitated in water and the polymer was isolated by decanting the solvent.

Functionalization of PCOE using mercaptopropionic acid

In a 20 ml vial, 750 mg of PCOE (M_n = 11,200 g/mol by ^{1}H NMR, 0.07 mmoles) was dissolved in 15 ml of THF at room temperature. The solution was degassed with an N_2 purge for 10 min after which mercaptopropionic acid (thiol to vinyl ratio ranging from 1:1 through 4:1) was added to the solution. After sparging with nitrogen for 5 more minutes, Irgacure 2959 (2 mol% relative to vinyl) was added to the solution. The reaction vial was sealed and stirred while exposed to UV-A light for either 120, 135, and 150 min to achieve different levels of functionalization. The reaction solution was then precipitated in water and the polymer was isolated by decanting the solvent.

Functionalization of PCOE using mercaptooctanoic acid

In a 100 ml round bottom flask, 750 mg of PCOE (M_n = 13,000 g/mol by ^{1}H NMR, 0.07 mmoles) was dissolved in 30 ml of THF at room temperature. The solution was degassed with a N_2 purge for 10 min after which mercaptooctanoic acid (thiol to vinyl ratio - 1:1) was added to the solution. After sparging with nitrogen for 5 more minutes, Irgacure 2959 (2 mol% relative to vinyl) was added to the solution. The reaction vial was sealed and stirred while exposed to UV-A light for 120 min to convert 36% of C=C. The reaction solution was then precipitated in water and the polymer was isolated by decanting the solvent.

In a 100 ml round bottom flask, 750 mg of PCOE (M_n = 13,000 g/mol by ^{1}H NMR, 0.07 mmoles) was dissolved in 50 ml of THF at room temperature. The solution was degassed with a N_2 purge for 10 min after which mercaptooctanoic acid (thiol to vinyl ratio - 4:1) was added to the solution. After sparging with nitrogen for 5 more minutes, Irgacure 2959 (4 mol% relative to vinyl input, 20 mg) was added to the solution. The photoinitiator was added by a dosing technique; 4 mol% of Irgacure 2959 was added every hour for 7 h to convert 84% of C=C. The reaction solution was precipitated in excess of methanol and the polymer was isolated by decanting the solvent.

Functionalized PCOE is denoted as *n*(*x*/4)-PCOE, where *n* represents the number of methylene groups in the pendant, *x* is the conversion of C=C bonds, and *x*/4 represents the functionalization determined by ^{1}H NMR, Fig. 1**b**. Functionalization refers to the fraction of ethylene monomeric units with a pendant group installed, and can range from 0 to 25%, when PCOE is the starting polymer.

Table 1

Conversion and COOH mass fraction determined by ^{1}H NMR as a function of thiol:vinyl ratio and reaction time. Number average molecular weight (M_n) was determined by end-group analysis in ^{1}H NMR. *denotes a sample was hydrogenated then functionalized.

	Thiol:vinyl Ratio	Reaction Time (min)	M_n (kg/mol)	Conversion (%)	COOH Mass Fraction
1h(3)-PCOE	2:1	15	10.9	12	0.04
1h(7)-PCOE	2:1	20	11.3	28	0.09
1h(13)-PCOE*	3:1	180	12.4	52	0.14
1h(16)-PCOE	2:1	60	14.8	64	0.17
1h(19)-PCOE	2:1	100	17.8	76	0.19
1h(22)-PCOE	2:1	120	19.1	88	0.21
2h(6)-PCOE	1:1	120	10.1	24	0.07
2h(11)-PCOE	2:1	120	11.3	44	0.12
2h(14)-PCOE	2.5:1	135	13.2	56	0.15
2h(17)-PCOE	3:1	120	11.2	68	0.17
2h(19)-PCOE	3.5:1	135	18.5	76	0.18
2h(22)-PCOE	4:1	120	23.2	88	0.19
7h(9)-PCOE	1:1	120	21.6	36	0.09
7h(21)-PCOE	4:1	420	32.8	84	0.15

Hydrogenation of functionalized PCOE

In a 250 ml round bottom flask, 600 mg of functionalized PCOE (M_n of initial PCOE – 11,200 g/mol or 13,000 g/mol) was dissolved in 30 ml of 1,1,2,2 tetrachloroethane (TCE). Samples with 12 mol% or more functionalization were too polar to dissolve in TCE. These samples were dissolved in 30 ml of DMSO. The round bottom flask was then transferred to an oil bath which was preheated to 125 °C. After letting the solution stir for 10 min, tri-*n*-propyl amine (5 molar excess of remaining unsaturation) was added to the solution. *Para*-toluene sulfonyl hydrazide (5 molar excess of remaining unsaturation) was then slowly added to the solution over 10 min and the reaction was stirred for 150 min. The hot solution was precipitated in methanol (ca. 300 ml). The presence of the base (tri-*n*-propyl amine) leads to formation of a carboxylate ammonium complex soluble in methanol. As a result, for samples with 12 mol% and higher functionalization, the precipitating solvent (methanol) was acidified using excess of 0.5 M HCl to crash the polymer out of the solution. Once the polymer is precipitated, the sample was isolated by decanting the solvent. After isolation, products with low levels of functionalization formed a powder while products with higher levels of functionalization formed a soft and tacky solid. Product was transferred to a vial and was dried under vacuum at 90 °C for 5 h. The polymers that are both functionalized and hydrogenated are referred to as *nh*(*x*/4)-PCOE, where *h* denotes complete hydrogenation. To account for differences in pendant length, samples are analyzed with respect to their COOH mass fraction, Table 1. We focused our studies on the hydrogenated forms of the functionalized polymers given in Table 1.

Hydrogenation followed by functionalization of PCOE

Partial hydrogenation

In a 250 ml round bottom flask, 750 mg of functionalized PCOE (M_n of initial PCOE – 11,200 g/mol) was dissolved in 40 ml of *p*-xylene at room temperature. The round bottom flask was transferred to an oil bath which was preheated to 125 °C. After letting the solution stir for 10 min, tri-*n*-propyl amine (5 molar excess of remaining unsaturation) was added to the solution. *Para*-toluene sulfonyl hydrazide (5 molar excess of remaining unsaturation) was then slowly added to the solution over 10 min. The reaction was stirred for 2.5 h. The hot solution was precipitated in methanol (ca. 300 ml) and the polymer was separated using gravity filtration. Polymer was a white powder suspended in hot water and recovered by decanting the solvent. Product was transferred to a vial and was dried under vacuum at 90 °C for 5 h.

Functionalization of the partially hydrogenated PCOE

In a 20 ml vial, 720 mg of the partially hydrogenated PCOE (M_n = 11,200 g/mol by ^{1}H NMR, 0.07 mmoles) was dissolved in 30 ml of THF at room temperature. The solution was degassed with a N_2 purge for 10 min after which thioglycolic acid (thiol to vinyl ratio 3:1) was added to the solution. After sparging with nitrogen for 5 more minutes, Irgacure 2959 (2 mol% relative to vinyl input, 30 mg) was added to the solution. The reaction vial was sealed and stirred while exposed to UV-A light for 180 min leading to 100% functionalization of remaining unsaturation. The reaction solution was then precipitated in water and the polymer was isolated by decanting the solvent.

Nuclear magnetic resonance (NMR) spectroscopy

^{1}H NMR spectroscopy of all functionalized samples were performed in 5 mm diameter tubes in deuterated chloroform ($CDCl_3$) at 25 °C on a Bruker 500 spectrometer at 500 MHz. ^{1}H NMR spectroscopy of the functionalized samples with $\leq$ 12 mol% functionalization (before and after hydrogenation) were performed with a Bruker Avance III 500 MHz NMR spectrometer in 1,1,2,2 tetrachloroethane-d_4 at room temperature. ^{1}H NMR spectroscopy of the functionalized samples with $>$ 12 mol% functionalization (before and after hydrogenation) were

performed with a Bruker Avance III 500 MHz NMR spectrometer in dimethyl sulfoxide-d_6 at room temperature. Diffusion-edited ^{1}H NMR spectroscopy removed residual solvent signals that overlapped with key resonances. ^{1}H NMR was used to calculate molar mass from end-group analysis, as described on page S7 and S8 in the supporting information section.

Contact angle measurements

Polymers were first dried in a vacuum oven at 125 °C for 5 h, high enough to melt the crystals but not hot enough to initiate anhydride formation between COOH groups [45]. This drying procedure was used before contact angle measurements, Fourier transform infrared spectroscopy (FTIR), X-ray scattering, differential scanning calorimetry (DSC), thermo-gravimetric analysis (TGA), and dynamic mechanical analysis (DMA). Polymer samples were hot pressed into flat circular films 1 cm in diameter. Hot pressing proceeded at 135 °C in a custom polytetrafluoroethylene (PTFE) window mold between two liners of PTFE and steel sheets. After a pre-heat for 5 min, polymers were pressed under one ton of pressure for an additional 15 min then allowed to return to room temperature. Water contact angle measurements were performed by applying a 10 μL droplet to the polymer surface then taking a picture in profile. The profile of the droplet was fit to the Young-Laplace eq. to identify the contact angle [46].

Fourier transform infrared spectroscopy (FTIR)

FTIR measurements were taken on a Nicolet is50 FTIR on an ATR attachment with a MCT/A liquid nitrogen cooled detector. Bulk polymer powder was compressed under an anvil against a diamond crystal. ATR-FTIR measurements were conducted at 0.2 cm^{-1} resolution and taken from the sum of 100 scans. FTIR absorbance spectra were normalized to the intensity of the C–H asymmetric peak at ~2850 cm^{-1}.

X-ray scattering

Approximately 2 mg of *n*h(*x*/4)-PCOE polymers were loaded into glass capillaries with diameters of 1 mm and wall thicknesses of 10 μm. X-ray scattering was performed on a Xeuss 2.0 instrument with a Cu Kα source. Small angle X-ray scattering (SAXS) data were collected by a 1 M Pilatus solid state detector and wide angle X-ray scattering (WAXS) data were collected by a 100 K Dectris detector. A Linkam I HFS350 stage controlled the sample temperature and X-ray scattering measurements were taken at both 25 and 125 °C. SAXS measurements were performed at a sample to detector distance (SD) of 576 mm and each exposure was taken with high flux collimation (slit 1 at 1.5 × 1.5 mm, slit 2 at 0.7 × 0.7 mm) for 30 min.

Differential scanning calorimetry (DSC)

Differential scanning calorimetry (DSC) was performed using a TA Q2000 instrument with ~ 5 mg of samples loaded into hermetic aluminum pans. DSC measurements were conducted in modulating mode with an amplitude of 1 K and period of 45 s. Samples were subjected to an initial heating to 150 °C to erase thermal history followed by a cooling then final heating cycle. The cooling and final heating cycles were conducted with a ramp rate of 5 K/min.

Thermo-gravimetric analysis (TGA)

Thermal gravimetric analysis (TGA) was performed using TA Instruments Q50 thermal gravimetric analyzer. TGA measurements were conducted on 5 mg of polymer loaded in a platinum pan and heated at 20 K/min from room temperature to 600 °C under a nitrogen atmosphere.

Dynamic mechanical analysis (DMA)

Samples were hot pressed into rectangular coupons of dimensions 25×3 × 0.5 mm using a custom stainless steel mold window mold following the same procedure described above in the contact angle section. A TA Instruments RSAIII was used for DMA measurements. DMA measurements were conducted as a function of temperature from −95 to 85 °C at a ramp rate of 5 K/min with a strain amplitude of 0.2% and a frequency of 1 Hz. The DMA automatically adjusted the average gap length between the crossbars to maintain a minimum load of 20 g to ensure sufficient signal. This strain amplitude lies within the linear elastic regime while producing enough force to generate sufficient signal, Fig. S21.

Results and discussions

Functionalization and hydrogenation from PCOE to nh-PCOE

Successful synthesis of *n*h(*x*/4)-PCOE was confirmed by diffusion edited ^{1}H NMR spectroscopy, Fig. 2**a**. Increase in functionalization is marked by an increase in the intensity of the thiolene methylene peak at δ = 3.1 ppm (1h-PCOE), 2.7 ppm (2h-PCOE) ppm, or 2.3 ppm (7h-PCOE) and the methine peak at δ = 2.6 ppm (1h-PCOE) or 2.9 ppm (2h-PCOE), Fig.s S1, S3, S5. ^{1}H NMR spectroscopy shows the successful hydrogenation of the samples denoted by the complete disappearance of the vinyl peak at δ = 5.4 ppm, Fig. 2**a**. The peaks corresponding to the functionalized material is still intact showing that the thiolene pendant group is unaffected by the hydrogenation reaction, Fig. S2, S4, S6. End group analysis in ^{1}H NMR shows the incorporation of pendant groups accounts for all changes in M_n (Table 1), demonstrating this polymer-to-polymer transformation retains the overall degree of polymerization.

Functionalization of 1h-PCOE was well controlled by reaction time, Fig. 2**b**. The functionalization of 1h-PCOE increases linearly with reaction time (r^2 = 0.97): from 3 mol% at 15 min to 22 mol% after 120 min. Similarly, the functionalization of 2h-PCOE was well controlled by reaction stoichiometry, Fig. 2**c**. Functionalization of 2h-PCOE increases linearly with the thiol to vinyl ratio (r^2 = 0.99); a 1:1 thiol to vinyl ratio yielded 5 mol% functionalization and a 4:1 thiol to vinyl ratio produced 22 mol% functionalization.

Partial hydrogenation then functionalization from PCOE to nh-PCOE

^{1}H NMR spectroscopy shows the reduced intensity in peaks corresponding to the vinyl and allyl region (δ = 5.4 and 2.0 ppm respectively) relative to the aliphatic region (δ = 1.3 ppm) confirming the partial hydrogenation of the PCOE sample, reducing the percent unsaturation from 25 mol% to 13 mol%, Fig. 3. Successful synthesis of the 1h-PCOE was confirmed using diffusion edited ^{1}H NMR characterization shown in Fig. 3 where

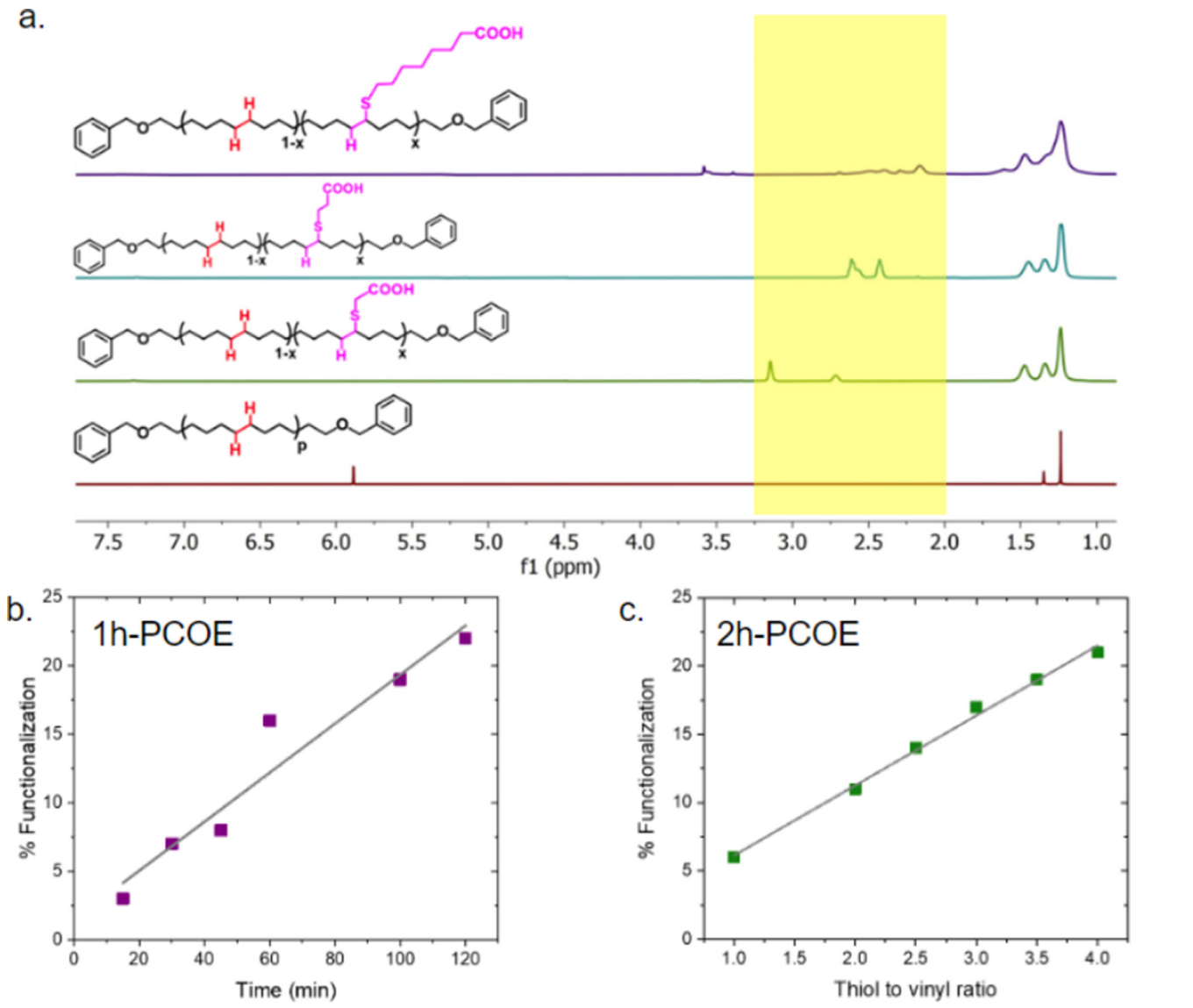

Fig. 2

(a) ^{1}H NMR of h-PCOE along with 1h(22)-PCOE, 2h(22)-PCOE, and 7h(21)-PCOE shifted vertically for clarity. The region highlighted in yellow contains the methylene and methine peaks that denote functionalization. Percent functionalization as determined by ^{1}H NMR of **(b)** 1h-PCOE functionalization controlled by reaction time and **(c)** 2h-PCOE functionalization controlled by thiol to vinyl ratio.

the vinyl peak at $\delta = 5.4$ ppm completely disappears and the thiolene methylene peak appears at $\delta = 3.2$ ppm and methine peak appears at $\delta = 2.9$ ppm.

Contact angle

The contact angle was determined by fitting the Young-Laplace eq. to an image of a water droplet on the surface, Fig. 4**.** The contact angle decreases from 98.1 ± 2.0 ° in h-PCOE to 62.3 ± 1.3° in 1h(22)-PCOE, indicating that the surface becomes more polar with greater acid incorporation. The contact angle does not strongly depend on pendant spacer when plotted as a function of COOH mass fraction, Fig. 4. The polymers reported here exhibit similar surface polarities to comparable commercial polymers as evidenced by the inclusion of commercial EAA contact angles. As contact angle measures surface polarity, a property crucial for adhesion, the polymers reported here show promise to plausibly replicate the adhesive properties of EAA.

FTIR

FTIR spectroscopy reveals the secondary bonding environment of COOH through shifts in the carboxylic acid C=O stretching peak. Numerical integration over the total C=O stretching region associated with COOH groups shows a strong relationship between the area of the COOH peak and COOH mass fraction as determined by ^{1}H NMR, Fig. 5**b**. When COOH groups do not participate in hydrogen bonding, the C=O stretching peak appears at ~ 1750 cm^{-1} [45,47]. A peak centered at ~ 1728 cm^{-1} is attributed to C=O stretch from COOH groups participating in one hydrogen bond and a peak at ~ 1705 cm^{-1} is attributed to COOH with two hydrogen bonds [45,47]. The COOH signals of *n*h(*x*/4)-

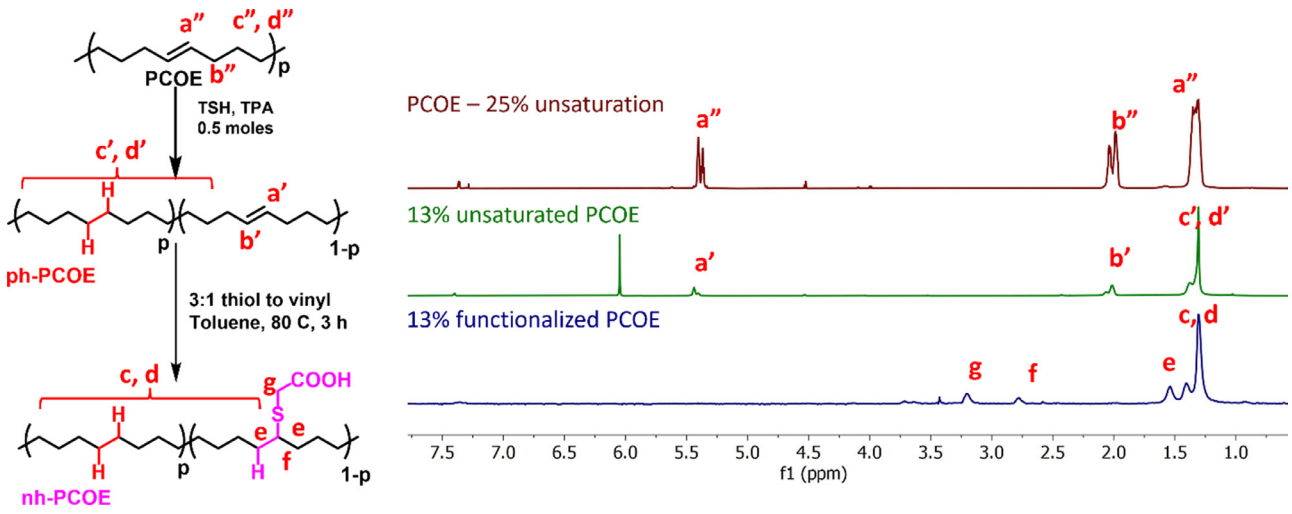

Fig. 3

Synthetic design for partially-hydrogenating PCOE then functionalizing the resulting product with thioglycolic acid. ^{1}H NMR spectra of the PCOE, partially-unsaturated PCOE, and 1h(13)-PCOE product showing successful partial hydrogenation then functionalization.

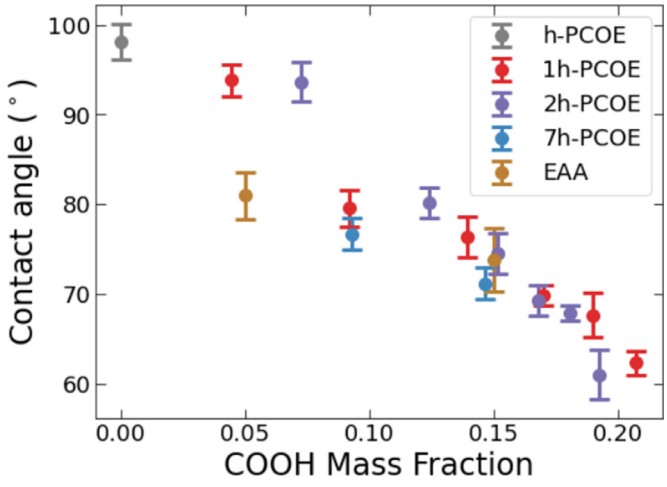

Fig. 4

Water contact angle from fitting the Young-Laplace eq. to a water droplet on room temperature on nh-PCOE surfaces.

PCOE polymers were fit to two Lorentzian functions, Fig. 5**a** [48]. These fits reveal > 95% of the COOH groups participate in either one or two hydrogen bonds. Integrating these peaks showed the fraction of COOH groups participating in two hydrogen bonds accounted for 56% to 100% of the total COOH signal in all polymers where fits were possible, Fig. S13.

X-ray scattering

While FTIR spectroscopy confirms that the COOH groups participate in hydrogen bonding, X-ray scattering detects aggregates of these hydrogen-bonded acid groups in 1h(*x*/4)-PCOE and 2h(*x*/4)-PCOE polymers, Fig. 6. 2D SAXS and WAXS patterns were isotropic and integrated azimuthally. The low Q peak in SAXS (Q ~ 0.4 $Å^{-1}$, ∇) is attributed to inter-aggregate scattering and is evident in 1h-PCOE with > 7 mol% functionalization, and 2h-PCOE with > 14 mol% functionalization, Fig. S14–16. Persistence of these peaks above the melting temperature, after the disappearance of all crystalline peaks, supports the assignment as inter-aggregate scattering. Heating the sample above the melting temperature slightly decreases the average inter-aggregate spacing by 0.5–1 Å (Table S1). This slight decrease matches observations in prior studies of the structure of COOH-containing precise polyolefins both above and below their melting temperatures [49,50].

These aggregates appear to have a liquid-like packing, as supported by the broad isotropic SAXS peak with no higher order reflections, and by prior investigations of precise EAA [29,39,40,49,51]. The peak broadness does not change with functionalization (Fig. S14–16), indicating that uniformity of interaggregate distances is independent of functionalization. This matches expectations for aggregate packing in precise acid-containing polyolefins [49,50]. Commercial EAA (random and branched) and random linear EAA polymers do not exhibit inter-aggregates scattering peaks due to the broader distribution of aggregate spacings [40,51]. The emergence of a detectable aggregate scattering peak as functionalization increases likely arises from both greater total signal and more regular periodicity of the polymer architecture.

X-ray scattering did not detect an inter-aggregate peak in 7h(21)-PCOE even though FTIR spectroscopy confirms the COOH groups participate in hydrogen bonding, because this polymer has a lower acid content than other highly functionalized samples given the longer pendant; 7h(21)-PCOE has an COOH mass fraction of ~ 0.15 compared to ~ 0.21 in 1h(22)-PCOE. Additionally, the longer pendant in 7h(*x*/4)-PCOE has more potential conformations than the other pendants studied, broadening the potential inter-aggregate spacing and possibly changing the aggregate shape. We observe an inter-aggregate scattering peak in 1h-PCOE but not 7h-PCOE at ~ 0.15 COOH mass fraction, evidencing the role of pendant alkane spacer in the detectable structure of *n*h(*x*/4)-PCOE polymers, Fig. 6**a**.

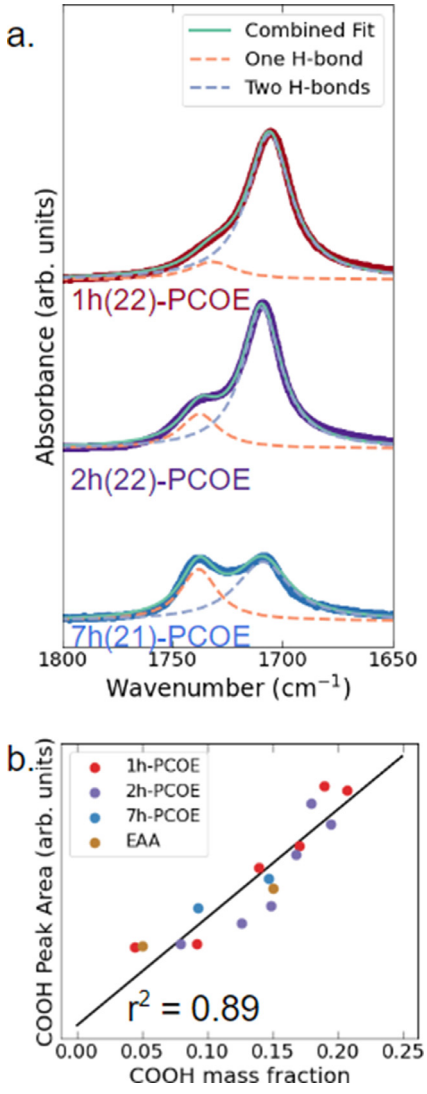

Fig. 5

(a) Representative FTIR spectra of the C=O stretch peak corresponding to COOH in 1h(22)-PCOE, 2h(22)-PCOE, and 7h(21)-PCOE with Lorentzian functions fit to the peaks from acids participating in one H-bond (~ 1728 cm^{-1}) and two H-bond (~ 1705 cm^{-1}) [45,47]. **(b)** The total integral of the COOH peak corresponds well to the COOH mass fraction measured by ^{1}H NMR.

The inter-aggregate spacing decreases with increasing COOH mass fraction, from ~ 24.8 Å at 9 wt% COOH to 15.5 Å at 20.7 wt% COOH (Fig. 6**b**). Atomistic molecular dynamics simulations of precise EAA show small acid aggregates of 2 or 3 acid groups nearly independent of COOH concentration [51,52]. Thus, increasing the COOH concentration generates more aggregates and decreases the inter-aggregate distances. Our observations match this intuition, as do prior investigations into acid containing polyolefins [29,39,40,49–51]. Inter-aggregate spacing of 1h-PCOE and 2h-PCOE polymers aligns with that of precise linear EAA synthesized by ADMET, Fig. 6**b** adapted from Seitz et al. [49]. This suggests the synthesis reported here offers an alternative route to pseudo-precise acid-containing polymers. When PCOE is fully functionalized, the pendant groups are separated by 6, 7, or 8 backbone carbons.

The sparsely-functionalized samples reported here exhibit crystallinity detectable by WAXS, 1h(3)-PCOE in Fig. 6**a** and S14–16. The WAXS scattering of *n*h(*x*/4)-PCOE polymers with < 14 wt% COOH have an orthorhombic crystal structure with lattice parameters of $a = 7.2$ Å and $b = 5.1$ Å, comparable to HDPE [53].

Thermal properties

DSC reveals a monotonic decrease in melting temperature, from 124 to 31 °C with increasing functionalization, Fig. 7**a**. This decrease in melting temperature is consistent with prior investigations of hydrogen bonding polymers and attributed to smaller crystallites [20,31,34,54]. The large pendant groups (≥ 73 g/mol) employed in this study to functionalize PCOE are not expected to incorporate into PE orthorhombic crystals and consequently decrease the crystallite size. Additionally, the decrease in melting temperature likely stems from a decrease in melting entropy as crystals completely reject pendant groups [54]. The melting temperature is also influenced by pendant spacer length; at similar mass fractions of COOH 2h-PCOE has a lower T_m than 1h-PCOE which in turn is lower than EAA. For example, the samples closest to 15 wt% COOH have T_m values of 83.1, 62.2, and 31.2 °C for commercial EAA, 1h(12)-PCOE, and 2h(11)-PCOE respectively.

Crystallinity was determined both by WAXS and DSC. By fitting the crystalline peaks to Lorentzian functions and the amorphous halo to a double Gaussian function (Fig. S17), we determined the fraction of total signal from crystalline scattering, a measure of crystallinity. WAXS confirms the semi-crystalline *n*h(*x*/4)-PCOE samples exhibit PE orthorhombic structure, so ΔH_m of 293 J/g was used to calculate percent crystallinity by DSC. The percent crystallinity measured by DSC corresponds well to WAXS, Fig. 7**b**. Moreover, crystallinity decreases with increasing functionalization from 56% in h-PCOE to no crystallinity at a COOH mass fraction of ~ 0.15 across all *n*h(*x*/4)-PCOE polymers, Fig. 7**b**. This decrease in crystallinity is well supported by prior investigations of acid-containing polymers [25–27,31,39]. This was also observed in our prior study on hydroxyl ether thioether functionalized PCOE [20].

Analysis of the samples using TGA revealed no significant peaks corresponding to small volatile molecules, indicating successful solvent removal and high sample purity following vacuum drying above T_m, Fig. S20. Importantly, COOH anhydride formation, C-S bond scission, and backbone degradation were measured by TGA and occur at expected values of ~ 200, ~ 350, and 450 °C respectively. These polymers exhibit good thermal stability, allowing for standard thermal processing.

Modulus and dynamics

Functionalizing PCOE with acid-terminated linear pendants tunes dynamic mechanical properties as investigated by temperature-sweep DMA measurements, Fig. 8**a-c**. The measured temperature range captures the glassy and rubbery plateaus in the storage modulus (E′) along with the glass transition, Fig. 8**a**. The glassy plateaus were determined from the E′ values 30 °C below the T_g. Note that in 1h(3)-PCOE at ~ 75 °C E′ starts to decrease, indicating melting. By comparison, the non-crystalline 1h(22)-PCOE does not exhibit a high temperature drop in the E′. Thus, the rubbery

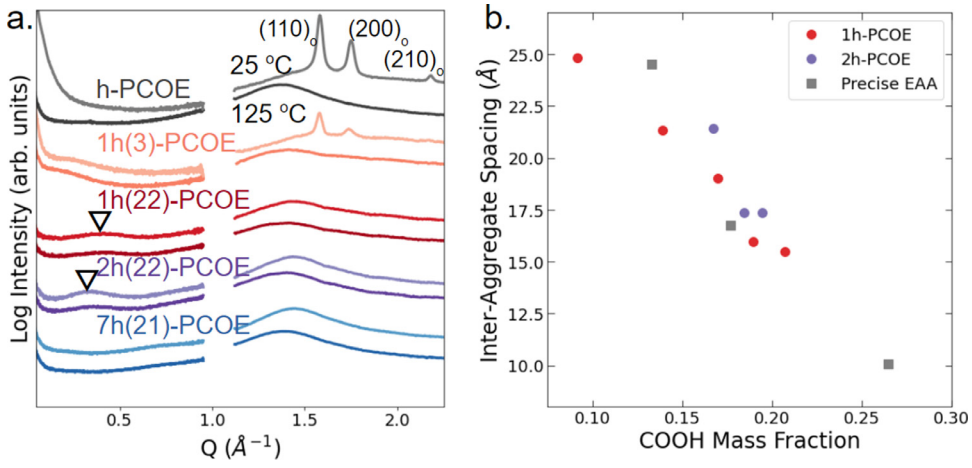

Fig. 6

(a) Representative X-ray scattering curves of *n*h(*x*/4)-PCOE samples showing both crystalline scattering at high Q in samples with < 14% functionality and inter-aggregate scattering (∇) at moderate Q for samples with higher acid fractions. **(b)** Inter-aggregate spacings for *n*h(*x*/4)-PCOE polymers with detectable inter-aggregate scattering peaks and the inter-aggregate spacing for precise linear EAA synthesized by ADMET [49].

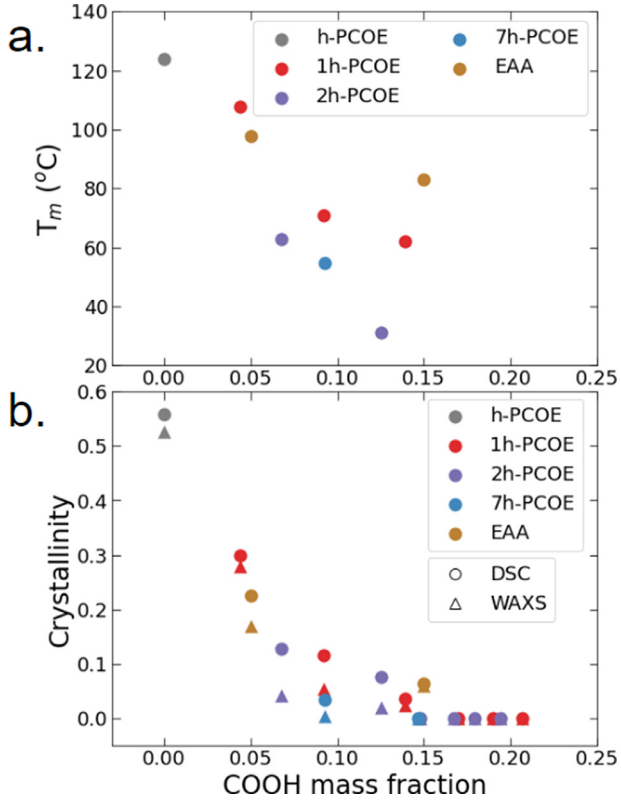

Fig. 7

(a) Melting temperature taken from melting endotherm on second heating at 5 K/min. **(b)** Crystallinity from WAXS at room temperature and enthalpy of melting divided by the enthalpy of melting of 100% crystalline orthorhombic PE (293 J/g).

E′ modulus was taken before the melting transition or at T_g + 30 °C, whichever is lower.

The glassy E′ plateau is independent of COOH fraction and pendant spacer, Fig. 8**b**, indicating that glassy dynamics are independent of concentration of acid group as controlled by either the level of functionalization or the pendant length. The glassy dynamics are largely dictated by the chain flexibility, so this result indicates that chain flexibility is independent of the COOH mass fraction [56]. This result matches observations from prior studies into acid containing polymers that show little changes in the glassy E′ with acid concentration [31]. However, the rubbery modulus shows a strong dependence on the COOH mass fraction, Fig. 8**b**. Both the glassy and rubbery plateau moduli of *n*h(*x*/4)-PCOE correspond well to commercial EAA.

Prior studies on acid-containing polymers also identified a decrease in rubbery modulus with greater acid incorporation, attributed to a loss of crystallinity [31,34]. Wakabayashi and Register successfully modeled the modulus of acid-containing polyolefins with the Davies model, treating the total modulus as a combination of amorphous and crystalline contributions normalized by the crystallinity [31,36]. Reductions in the crystallinity decreases the contribution from the much stiffer crystalline phase. Indeed, crystallinity decreases in *n*h(*x*/4)-PCOE polymers as a function of COOH incorporation. However, at ~ 0.15 COOH mass fraction, crystallinity completely disappears but the rubbery E′ plateau continues to decrease. Thus these materials fail to meet the assumption of the Davies model that the amorphous modulus is independent of the acid fraction.

Alternatively, Fetters et al. described the polyolefin plateau shear storage moduli as a function of the average molecular weight per backbone bond (m_b) [55,57,58]. This backbone equivalence model posits that extra free volume and the increased packing length inherent with side-chains reduce the entanglement (or rubbery) plateau storage modulus as compared to a linear polyolefin. From Bueche-Rouse, Fetters et al. determined a theoretical relationship between the modulus and the parameter m_b (eq. (1)) [55,59].

$$G'_{rubbery} = \left(\frac{14}{m_b}\right)^3 G'_{linear} \sim m_b^{-3} \quad (1)$$

Applying this theory to experimental measurements of branched polyolefins revealed two regimes, a lightly branched

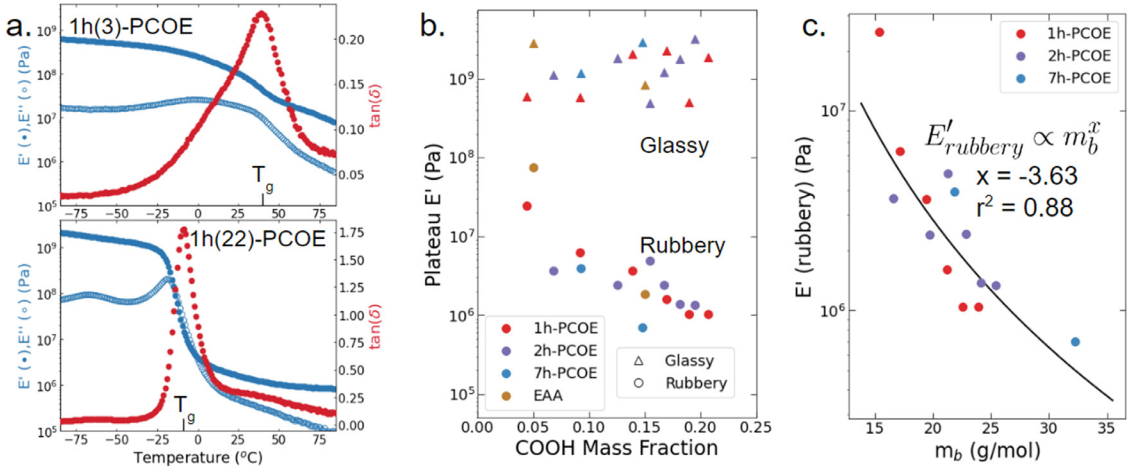

Fig. 8

(a) Representative DMA temperature sweeps for 1h(3)-PCOE and 1h(22)-PCOE taken from −95 to 85 °C with a heating rate of 5 K/min, a strain rate of 1 Hz, and fixed strain amplitude of 0.2 %. **(b)** Glassy (triangles) and rubbery (circles) plateau moduli respectively. **(c)** The rubbery plateau modulus fit to the backbone equivalence model [55].

regime described by $G'_{rubbery} \sim m_b^{-3.49}$ and a higher branched regime described by $G'_{rubbery} \sim m_b^{-1.58}$ [55]. Follow-up studies on well controlled bottlebrush polymers found exponents of −3 for the lightly branched regime along with −1.5 and −1.47 for the heavily branched regime [57,58]. Liang et al. further explored the relationship between side chain density, length, and resulting entanglement plateau modulus in polyolefins with n–butyl acrylate pendants [57]. They show that the exponential relationship between the rubbery plateau modulus and m_b extends to polymers with chemically different backbone and side chains.

Thus, we apply the backbone equivalence model to the *n*h(*x*/4)-PCOE polymers reported here, and find it fits the rubbery modulus with an exponent of −3.63, Fig. 8**c**. This exponent is in good agreement with both Fetters et al. and Liang et al. [55,57]. We attribute the decrease in rubbery modulus with increasing acid fraction to both a loss of crystallinity and an increase in packing length due to the short chain branching character of the pendant groups in our three *n*h(*x*/4)-PCOE polymers. We attribute deviation from an exponent of −3 to the presence of acid aggregates that act as physical crosslinks, which the backbone equivalence model omits.

Prior studies of conventional acid-containing polymers reveal an increase in T_g with increasing acid fraction [30–32]. Indeed, our measurements of commercial EAA show a ~ 20 °C increase in T_g when the COOH mass fraction increases from 5 to 15 wt%, Fig. 9. In contrast, the glass transition temperatures of *n*h(*x*/4)-PCOE decrease with higher acid fraction, as measured by both DMA and DSC, Fig. 9. This T_g behavior likely stems from the confluence of two phenomena with opposite effects on T_g. First, reduced polymer mobility around acid aggregates as compared to EAA. Secondly, an increase in free volume associated with short-chain branching [29,41,60]. Prior studies of polyolefins with short-chain branching showed that T_g decreased as a function of side-chain fraction [58,60].

Interestingly, DMA detects multiple glass transitions at COOH mass fractions above ~ 0.09 for 1h(*x*/4)-PCOE and ~ 0.15 for 2h(*x*/4)-PCOE and 7h(*x*/4)-PCOE, Fig. 9. Though expected for ionomers, multiple glass transitions have not been observed in conventional acid-containing polymers [30,61,62]. Fully understanding both this lower temperature relaxation and the trend in T_g requires a more thorough investigation into polymer dynamics, which is ongoing.

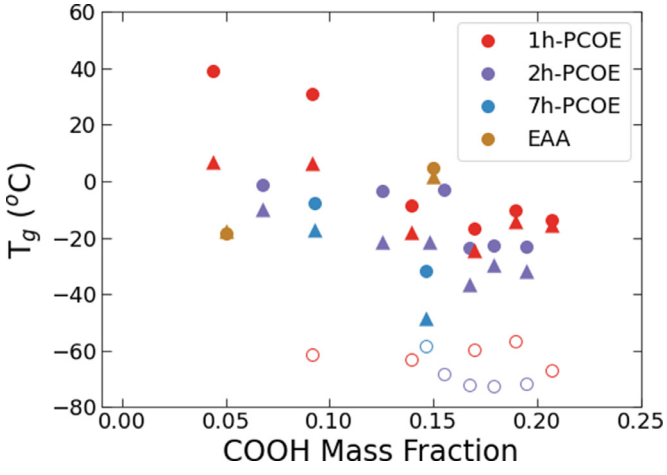

Fig. 9

Glass transition temperature taken from the reversing heat flow upon cooling in modulated DSC (triangles) and peaks in the tan(δ) signal in temperature-sweep DMA (circles). Open circles represent lower temperature T_g detected by DMA.

Conclusions

We successfully functionalized PCOE with three acid-terminated linear pendants and demonstrated excellent control of the reaction using both reaction stoichiometry and time. This versatile chemistry also works on polyolefins with lower levels of unsaturation than PCOE and avoids the need to protect the acid groups. We establish how the COOH mass fraction, as controlled by the number of functional groups and the

length of the pendant group, impacts the morphological, surface, thermal, and dynamic mechanical properties. Note that residual unsaturated carbon-carbon bonds in partially functionalized PCOE were removed by hydrogenation (functionalize then hydrogenate). Alternatively, a partially hydrogenated PCOE was fully functionalized (hydrogenate then functionalize), so that all materials tested are free of C=C bonds. Due to the expected randomness of these reactions, we expect that both routes produce comparable materials at fixed COOH mass fraction, though this is an opportunity for a future investigation.

The inclusion of COOH groups increases the surface polarity of the *n*h(*x*/4)-PCOE polymers at greater acid fractions and corresponds well to commercial EAA. FTIR spectroscopy reveals the attached COOH groups primarily participate in two hydrogen bonds. We observe the resulting acid aggregates via X-ray scattering, and find they correlate well to COOH mass fraction. Crystallinity and T_m decrease with greater COOH mass fraction and longer pendants further reduce T_m. Higher COOH mass fraction reduces the rubbery plateau modulus while the glassy modulus is independent of both acid fraction and pendant length, as determined by DMA. Both the rubbery and glassy plateau moduli of *n*h(*x*/4)-PCOE correspond well to EAA. The backbone equivalence model, that relates the rubbery plateau modulus to m_b, describes the rubbery modulus of *n*h(*x*/4)-PCOE polymers well by $E' \sim m_b^{-3.63}$. Interestingly, the *n*h(*x*/4)-PCOE polymers do not exhibit the expected increase in T_g with COOH mass fraction. Additionally, DMA detects multiple glass transitions in highly functionalized *n*h(*x*/4)-PCOE polymers.

By extending our previously-reported thiol-ene click chemistry to functionalize PCOE with three different acid-terminated linear pendants, we further advance the strategy for polymer-to-polymer upcycling by dehydrogenation then functionalization of polyolefins. In previous work, we used thiol-ene click chemistry to functionalize PCOE with OH and generate a suitable substitute for poly(ethylene-co-vinyl alcohol) [20]. Here we elaborate on that polymer chemistry to produce *n*h(*x*/4)-PCOE polymers with commensurate surface and mechanical properties to commercial EAA, demonstrating promise for packaging and adhesive applications. Moreover, these COOH functionalized polymers could be neutralized with metal cations to produce ionomers and further extend properties. We envision this versatile chemistry as a platform for reducing polyolefin waste and synthesizing specialty polymers.

Associated content

Supporting information contains additional experimental details along with measurements of each polymer by: ^{1}H NMR, FTIR, X-ray scattering, DSC, TGA, and DMA.

Declaration of competing interest

The authors declare that they have no known competing financial interests or personal relationships that could have appeared to influence the work reported in this paper.

Data availability

Data will be made available on request.

CRediT authorship contribution statement

Eli Fastow: Data curation, Formal analysis, Investigation, Methodology, Visualization, Writing – original draft. **Roshni John Chethalen:** Data curation, Formal analysis, Investigation, Methodology, Visualization, Writing – original draft. **E. Bryan Coughlin:** Conceptualization, Funding acquisition, Supervision, Writing – review & editing. **Karen I. Winey:** Conceptualization, Funding acquisition, Project administration, Supervision, Writing – review & editing.

Acknowledgements

The authors gratefully acknowledge funding by DOE BES (DESC0022238). The authors also wish to acknowledge Prof. Russ Composto for the use of his contact angle measurement system, Prof. Cherie Kagan for the use of her FTIR, Steve Szewczyk for his assistance with the DSC and DMA systems, James Votruba-Drzal for taking FTIR of EAA samples, and Dr. Weiguo Hu for assistance with acquiring NMR spectra. E.J.F. and K.I.W. acknowledge use of the Dual Source and Environmental X-ray Scattering facility operated by the Laboratory for Research on the Structure of Matter at the University of Pennsylvania supported by NSF through DMR-2309043 grant. E.J.F. acknowledges support from the Vagelos Institute of Energy Sciences and Technology in the form of a graduate fellowship.

Supplementary materials

Supplementary material associated with this article can be found, in the online version, at doi:10.1016/j.giant.2023.100231.

References

[1] B.D. Vogt, K.K. Stokes, S.K. Kumar, Why is recycling of postconsumer plastics so challenging? ACS Appl. Polym. Mater. (2021), doi:10.1021/acsapm.1c00648.

[2] The New Plastics Economy — Rethinking the future of plastics. World Economic Forum, Ellen MacArthur Foundation and McKinsey & Company; 2016.

[3] R. Geyer, J.R. Jambeck, K.L. Law, Production, use, and fate of all plastics ever made, Sci. Adv. (2017), doi:10.1126/sciadv.1700782.

[4] S. Billiet, S.R. Trenor, 100th anniversary of macromolecular science viewpoint: needs for plastics packaging circularity, ACS Macro Lett. 9 (2020) 1376–1390, doi:10.1021/acsmacrolett.0c00437.

[5] H. Li, H.A. Aguirre-Villegas, R.D. Allen, X. Bai, C.H. Benson, G.T. Beckham, et al., Expanding plastics recycling technologies: chemical aspects, Technol. Status Challenges (2022), doi:10.26434/chemrxiv-2022-9wqz0.

[6] H. Hinsken, S. Moss, J.R. Pauquet, H. Zweifel, Degradation of polyolefins during melt processing, Polym. Degrad. Stab. 34 (1991) 279–293, doi:10.1016/0141-3910(91)90123-9.

[7] J. Zheng, S. Suh, Strategies to reduce the global carbon footprint of plastics, Nat. Clim. Chang. 9 (2019) 374–378, doi:10.1038/s41558-019-0459-z.

[8] X. Li, J. Wang, T. Zhang, S. Yang, M. Sun, X. Qian, et al., Sustainable catalytic strategies for the transformation of plastic wastes into valued products, Chem. Eng. Sci. (2023) 118729, doi:10.1016/j.ces.2023.118729.

[9] J.B. Williamson, S.E. Lewis, R.R. Johnson, I.M. Manning, Leibfarth FA. C–H functionalization of commodity polymers, Angew. Chem. Int. Ed. 58 (2019) 8654–8668, doi:10.1002/anie.201810970.

[10] J.B. Williamson, W.L. Czaplyski, E.J. Alexanian, F.A. Leibfarth, Regioselective C–H xanthylation as a platform for polyolefin functionalization, Angew. Chem. Int. Ed. 57 (2018) 6261–6265, doi:10.1002/anie.201803020.

[11] M. Zeng, Y.H. Lee, G. Strong, A.M. LaPointe, A.L. Kocen, Z. Qu, et al., Chemical upcycling of polyethylene to value-added α,ω-divinyl-functionalized oligomers, ACS Sustain Chem. Eng. (2021), doi:10.1021/acssuschemeng.1c05272.

[12] M. Zhang, R.H. Colby, S.T. Milner, T.C.M. Chung, T. Huang, W deGroot, Synthesis and characterization of maleic anhydride grafted polypropylene with a well-defined molecular structure, Macromolecules 46 (2013) 4313–4323, doi:10.1021/ma4006632.

[13] L. Chen, K.G. Malollari, A. Uliana, D. Sanchez, P.B. Messersmith, Hartwig JF. Selective, Catalytic oxidations of C–H bonds in polyethylenes produce functional materials with enhanced adhesion, Chem. 7 (2021) 137–145, doi:10.1016/j.chempr.2020.11.020.

[14] A. Ray, K. Zhu, Y.V. Kissin, A.E. Cherian, G.W. Coates, A.S. Goldman, Dehydrogenation of aliphatic polyolefins catalyzed by pincer-ligated iridium complexes, Chem. Commun. (2005) 3388–3390, doi:10.1039/B502120K.

[15] A. Ray, Y.V. Kissin, K. Zhu, A.S. Goldman, A.E. Cherian, G.W. Coates, Catalytic post-modification of alkene polymers: chemistry and kinetics of dehydrogenation of alkene polymers and oligomers with pincer Ir complexes, J. Mol. Catal. A Chem. 256 (2006) 200–207, doi:10.1016/j.molcata.2006.04.017.

[16] K. Zhu, P.D. Achord, X. Zhang, K. Krogh-Jespersen, A.S. Goldman, Highly effective pincer-ligated iridium catalysts for alkane dehydrogenation. DFT calculations of relevant thermodynamic, kinetic, and spectroscopic properties, J. Am. Chem. Soc. 126 (2004) 13044–13053, doi:10.1021/ja047356l.

[17] R.J. Conk, S. Hanna, J.X. Shi, J. Yang, N.R. Ciccia, L. Qi, et al., Catalytic deconstruction of waste polyethylene with ethylene to form propylene, Science 377 (2022) 1561–1566, doi:10.1126/science.add1088.

[18] N.M. Wang, G. Strong, V. DaSilva, L. Gao, R. Huacuja, I.A. Konstantinov, et al., Chemical recycling of polyethylene by tandem catalytic conversion to propylene, J. Am. Chem. Soc. 144 (2022) 18526–18531, doi:10.1021/jacs.2c07781.

[19] L.D. Ellis, S.V. Orski, G.A. Kenlaw, A.G. Norman, K.L. Beers, Y. Román-Leshkov, et al., Tandem heterogeneous catalysis for polyethylene depolymerization via an olefin-intermediate process, ACS Sustain Chem. Eng. 9 (2021) 623–628, doi:10.1021/acssuschemeng.0c07612.

[20] R.J. Chethalen, E.J. Fastow, E.B. Coughlin, K.I. Winey, Thiol–ene click chemistry incorporates hydroxyl functionality on polycyclooctene to tune properties, ACS Macro Lett. 12 (2023) 107–112, doi:10.1021/acsmacrolett.2c00670.

[21] V.A. Tanna, J.S. Enokida, E.B. Coughlin, H.H. Winter, Functionalized polybutadiene for clay–polymer nanocomposite fabrication, Macromolecules 52 (2019) 6135–6141, doi:10.1021/acs.macromol.9b00616.

[22] C.E. Hoyle, C.N. Bowman, Thiol-Ene click chemistry, Angew. Chem. Int. Ed. 49 (2010) 1540–1573, doi:10.1002/anie.200903924.

[23] S. Kim, M.A. Rahman, M. Arifuzzaman, D.B. Gilmer, B. Li, J.K. Wilt, et al., Closed-loop additive manufacturing of upcycled commodity plastic through dynamic cross-linking, Sci. Adv. 8 (2022) eabn6006, doi:10.1126/sciadv.abn6006.

[24] A. Eisenberg, J.S. Kim, Introduction to Ionomers, Wiley, 1998.

[25] R.C. Scogna, R.A. Register, Plastic deformation of ethylene/methacrylic acid copolymers and ionomers, J. Polym. Sci. Part B Polym. Phys. 47 (2009) 1588–1598, doi:10.1002/polb.21762.

[26] W.J. MacKnight, T.R Earnest Jr, The structure and properties of ionomers, J. Polymer Sci. 16 (1981) 41–122, doi:10.1002/pol.1981.230160102.

[27] W.J. MacKnight, L.W. McKenna, B.E. Read, Properties of ethylene-methacrylic acid copolymers and their sodium salts: mechanical relaxations, J. Appl. Phys. 38 (1967) 4208–4212, doi:10.1063/1.1709106.

[28] S. Deschanel, B.P. Greviskes, K. Bertoldi, S.S. Sarva, W. Chen, S.L. Samuels, et al., Rate dependent finite deformation stress–strain behavior of an ethylene methacrylic acid copolymer and an ethylene methacrylic acid butyl acrylate copolymer, Polymer (Guildf) 50 (2009) 227–235, doi:10.1016/j.polymer.2008.10.049.

[29] L.R. Middleton, K.I. Winey, Nanoscale aggregation in acid- and ion-containing polymers, Annu. Rev. Chem. Biomol. Eng. 8 (2017) 499–523, doi:10.1146/annurev-chembioeng-060816-101531.

[30] R.C. Scogna, R.A. Register, Yielding in ethylene/methacrylic acid ionomers, Polymer (Guildf) 50 (2009) 585–590, doi:10.1016/j.polymer.2008.12.003.

[31] K. Wakabayashi, R.A. Register, Micromechanical interpretation of the modulus of ethylene–(meth)acrylic acid copolymers, Polymer (Guildf) 46 (2005) 8838–8845, doi:10.1016/j.polymer.2004.12.063.

[32] H. Matsuura, A. Eisenberg, Glass transitions of ethyl acrylate-based ionomers, J. Polymer Sci. 14 (1976) 1201–1209, doi:10.1002/pol.1976.180140705.

[33] T. Tomkovic, S.G. Hatzikiriakos, Nonlinear rheology of poly(ethylene-co-methacrylic acid) ionomers, J. Rheol. 62 (2018) 1319–1329, doi:10.1122/1.5042521.

[34] S.E. Lehman, K.B. Wagener, L.S. Baugh, S.P. Rucker, D.N. Schulz, M. Varma-Nair, et al., Linear copolymers of ethylene and polar vinyl monomers via olefin metathesis−hydrogenation: synthesis, characterization, and comparison to branched analogues, Macromolecules 40 (2007) 2643–2656, doi:10.1021/ma070085p.

[35] E. Pregi, D. Kun, A. Wacha, B. Pukánszky, The role of ionic clusters in the determination of the properties of partially neutralized ethylene-acrylic acid ionomers, Eur. Polym. J. 142 (2021) 110110, doi:10.1016/j.eurpolymj.2020.110110.

[36] W.E.A. Davies, The theory of elastic composite materials, J. Phys. D Appl. Phys. 4 (1971) 1325–1339, doi:10.1088/0022-3727/4/9/313.

[37] T.W. Baughman, C.D. Chan, K.I. Winey, K.B. Wagener, Synthesis and morphology of well-defined poly(ethylene- co -acrylic acid) copolymers, Macromolecules 40 (2007) 6564–6571, doi:10.1021/ma070841r.

[38] B.S. Aitken, C.F. Buitrago, J.D. Heffley, M. Lee, H.W. Gibson, K.I. Winey, et al., Precision ionomers: synthesis and thermal/mechanical characterization, Macromolecules 45 (2012) 681–687, doi:10.1021/ma202304s.

[39] L.R. Middleton, S. Szewczyk, J. Azoulay, D. Murtagh, G. Rojas, K.B. Wagener, et al., Hierarchical acrylic acid aggregate morphologies produce strain-hardening in precise polyethylene-based copolymers, Macromolecules 48 (2015) 3713–3724, doi:10.1021/acs.macromol.5b00797.

[40] L.R. Middleton, E.B. Trigg, E. Schwartz, K.L. Opper, T.W. Baughman, K.B. Wagener, et al., Role of periodicity and acid chemistry on the morphological evolution and strength in precise polyethylenes, Macromolecules 49 (2016) 8209–8218, doi:10.1021/acs.macromol.6b00937.

[41] L.R. Middleton, J.D. Tarver, J. Cordaro, M. Tyagi, C.L. Soles, A.L. Frischknecht, et al., Heterogeneous chain dynamics and aggregate lifetimes in precise acid-containing polyethylenes: experiments and simulations, Macromolecules 49 (2016) 9176–9185, doi:10.1021/acs.macromol.6b01918.

[42] E.B. Trigg, L.R. Middleton, L. Yan, K.I. Winey, Comparing morphological evolution during tensile deformation of two precise polyethylenes via 2D fitting of in situ X-ray scattering, Macromolecules 51 (2018) 7942–7950, doi:10.1021/acs.macromol.8b01639.

[43] T. Rünzi, D. Fröhlich, S. Mecking, Direct synthesis of ethylene−acrylic acid copolymers by insertion polymerization, J. Am. Chem. Soc. 132 (2010) 17690–17691, doi:10.1021/ja109194r.

[44] C. Meyer, O. Pascui, D. Reichert, L.C. Sander, S.A. Wise, K. Albert, Conformational temperature dependence of a poly(ethylene-co-acrylic acid) stationary phase investigated by nuclear magnetic resonance spectroscopy and liquid chromatography, J. Sep. Sci. 29 (2006) 820–828, doi:10.1002/jssc.200500376.

[45] J.Y. Lee, P.C. Painter, M.M. Coleman, Hydrogen bonding in polymer blends. 3. Blends involving polymers containing methacrylic acid and ether groups, Macromolecules 21 (1988) 346–354, doi:10.1021/ma00180a011.

[46] F.J. Stadler, C. Bailly, A new method for the calculation of continuous relaxation spectra from dynamic-mechanical data, Rheol. Acta 48 (2009) 33–49, doi:10.1007/s00397-008-0303-2.

[47] M.M. Coleman, P.C. Painter, Hydrogen bonded polymer blends, Prog. Polym. Sci. 20 (1995) 1–59, doi:10.1016/0079-6700(94)00038-4.

[48] C. Sandt, J. Waeytens, A. Deniset-Besseau, C. Nielsen-Leroux, A. Réjasse, Use and misuse of FTIR spectroscopy for studying the bio-oxidation of plastics, Spectrochim. Acta Part A 258 (2021) 119841, doi:10.1016/j.saa.2021.119841.

[49] M.E. Seitz, C.D. Chan, K.L. Opper, T.W. Baughman, K.B. Wagener, K.I. Winey, Nanoscale morphology in precisely sequenced poly(ethylene-co-acrylic acid) zinc ionomers, J. Am. Chem. Soc. 132 (2010) 8165–8174, doi:10.1021/ja101991d.

[50] C.F. Buitrago, T.M. Alam, K.L. Opper, B.S. Aitken, K.B. Wagener, K.I. Winey, Morphological trends in precise acid- and ion-containing polyethylenes at elevated temperature, Macromolecules 46 (2013) 8995–9002, doi:10.1021/ma4013175.

[51] C.F. Buitrago, D.S. Bolintineanu, M.E. Seitz, K.L. Opper, K.B. Wagener, M.J. Stevens, et al., Direct comparisons of X-ray scattering and atomistic molecular dynamics simulations for precise acid copolymers and ionomers, Macromolecules 48 (2015) 1210–1220, doi:10.1021/ma5022117.

[52] C.A. Lueth, D.S. Bolintineanu, M.J. Stevens, A.L. Frischknecht, Hydrogen-bonded aggregates in precise acid copolymers, J. Chem. Phys. 140 (2014) 054902, doi:10.1063/1.4863326.

[53] C.W. Bunn, T.C. Alcock, The texture of polythene, Trans. Faraday Soc. 41 (1945) 317, doi:10.1039/tf9454100317.

[54] B. Crist, Thermodynamics of statistical copolymer melting, Polymer (Guildf) 44 (2003) 4563–4572, doi:10.1016/S0032-3861(03)00331-8.

[55] L.J. Fetters, D.J. Lohse, C.A. García-Franco, P. Brant, D. Richter, Prediction of melt state poly(α-olefin) rheological properties: the unsuspected role of the average molecular weight per backbone bond, Macromolecules 35 (2002) 10096–10101, doi:10.1021/ma025659z.

[56] P.B. Bowden, The elastic modulus of an amorphous glassy polymer, Polymer (Guildf) 9 (1968) 449–454, doi:10.1016/0032-3861(68)90054-2.

[57] H. Liang, B.J. Morgan, G. Xie, M.R. Martinez, E.B. Zhulina, K. Matyjaszewski, et al., Universality of the entanglement plateau modulus of comb and bottlebrush polymer melts, Macromolecules 51 (2018) 10028–10039, doi:10.1021/acs.macromol.8b01761.

[58] C.R. López-Barrón, A.H. Tsou, J.R. Hagadorn, J.A. Throckmorton, Highly entangled α-olefin molecular bottlebrushes: melt structure, linear rheology, and interchain friction mechanism, Macromolecules 51 (2018) 6958–6966, doi:10.1021/acs.macromol.8b01431.

[59] Bueche F. Viscosity, Self-Diffusion, and allied effects in solid polymers, J. Chem. Phys. 20 (2004) 1959–1964, doi:10.1063/1.1700349.

[60] X. Luo, S. Xie, J. Liu, H. Hu, J. Jiang, W. Huang, et al., The relationship between the degree of branching and glass transition temperature of branched polyethylene: experiment and simulation, Polym. Chem. 5 (2014) 1305–1312, doi:10.1039/C3PY00896G.

[61] B. Hird, A. Eisenberg, Phase dominance, multiple glass transitions, and apparent activation energies in some poly (styrene-co-alkali methacrylate) ionomers, J. Polym. Sci. Part B Polym. Phys. 28 (1990) 1665–1675, doi:10.1002/polb.1990.090281002.

[62] A. Eisenberg, B. Hird, R.B. Moore, A new multiplet-cluster model for the morphology of random ionomers, Macromolecules 23 (1990) 4098–4107, doi:10.1021/ma00220a012.